Aging dynamics of colloidal hard sphere glasses

Aging dynamics of colloidal hard sphere glasses

V. A. Martinez,[a] G. Bryant, and W. van Megen[b]
Department of Applied Physics, Royal Melbourne Institute of Technology, Melbourne, Victoria 3000, Australia

(Received 20 May 2010; accepted 21 July 2010; published online 21 September 2010)

We report the results of dynamic light scattering measurements of the coherent intermediate scattering function (ISF) of glasses of colloidal hard spheres for several volume fractions and a range of scattering vectors around the primary peak of the static structure factor. The ISF shows a clear crossover from an initial fast decay to a slower nonstationary decay. Aging is quantified in several different ways. However, regardless of the method chosen, the perfect "aged" glass is approached in a power law fashion. In particular the coupling between the fast and slow decays, as measured by the degree of stretching of the ISF at the crossover, also decreases algebraically with waiting time. The nonstationarity of this coupling implies that even the fastest detectable processes are themselves nonstationary. © *2010 American Institute of Physics*. [doi:10.1063/1.3478542]

I. INTRODUCTION

Aging—the nonstationary dynamics of deeply quenched fluids—has been a subject of considerable investigation over the past decade. Examples of materials that have been studied recently include sponges, foams and polymer and colloidal gels.[1] Unlike window glass and obsidian, these mesoscopic, soft complex materials lend themselves particularly well to the study of aging. Their nonstationary structural dynamics are commonly exposed by the dependence of the correlation function of density fluctuations [the intermediate scattering function (ISF)] on the waiting time. Despite the diversity and complexity illustrated by these examples, their dynamics share several features: An initial fast decay of the ISF to a plateau is followed by a slower decay. The initial decay is observed to be independent of age, while the decay from the plateau is observed to slow as the material ages. The fact that this slow decay follows a compressed exponential function of the delay time suggests an underlying very slow ballistic, rather than diffusive, motion. Indeed, these features have been attributed to elastic deformation driven by the evolution or redistribution of stresses, such as occurs in the shrinkage of gels and coarsening of foams.[2]

Stationarity of the fast process and scaling of the slow, nonstationary decay with waiting time are the two aspects that these experimental observations share with the results of numerous computer simulations of simple molecular glasses.[3,4] The difference is that the ISFs of the molecular glasses tend to decay algebraically from their respective plateaux; Here quenched-in stresses appear to be relieved through cooperative, avalanchelike events.[3]

A suspension of particles with hard sphere-like interactions presents a simpler experimental system. The interactions between the particles, deriving from thin solvated oligomeric surface layers, are effectively ageless. Provided the spread of particle radii is not too large—less than about 10% of their mean—these suspensions show a transition from a disordered, fluidlike phase to an opalescent, crystal phase that mimics the freezing-melting transition of simple atomic materials.[5] They also show a glass transition (GT), identified by the particle concentration where density fluctuations fail to fully relax on any reasonable experimental time scale.[6] Even in the context of the GT, the existence of the first order transition, in that it provides a thermodynamic reference for locating the undercooled, nonequilibrium states, remains pivotal.

When the glass of colloidal hard spheres was first observed, its aging was not exposed due, in no small part, to the limited understanding of how to deal experimentally with nonergodicity and nonstationarity. The light scattering procedures developed at the time to account for nonergodicity assumed stationarity.[6,7] In that sense, the colloidal glass was considered ideal. Indeed, the transition from colloidal fluid to the glass still appears to be the best experimental illustration of the sharp transition predicted by the idealized version of mode-coupling theory (MCT) (Ref. 8), a view reinforced by quantitative consistency between MCT and results of dynamic light scattering (DLS) experiments for these colloidal systems.[9,10] Neglect of those irreversible, ergodicity restoring processes, processes so much more vigorous in molecular glass formers than in colloidal systems, is generally considered to be the theory's main shortcoming.[11] The incorporation of such processes necessarily requires the introduction of further approximations and assumptions. However, by comparison with experiment the idealized theory can also be exploited to aid in quantifying the very processes it neglects.[10,12]

The first technique by which a statistically viable ensemble of density fluctuations, having decay times longer than the measurement time, could be accumulated with a sufficient speed to resolve slow, nonstationary processes was introduced by Müller and Palberg[13] in 1996. When this technique was subsequently applied to the glass of colloidal hard

[a]Present address: SUPA and School of Physics and Astronomy, The University of Edinburgh, Mayfield Road, Edinburgh EH9 3JZ, United Kingdom.
[b]Electronic mail: bill.vanmegen@rmit.edu.au.

TABLE I. Volume fractions (ϕ and ϕ_p, respectively, referenced to the freezing values of the one component and polydisperse hard sphere system), separation parameter ε, and scattering vectors qR for the two types of particle used in these experiments, specified by radius R, polydispersity σ, and Brownian time τ_b.

Suspension	ϕ	ϕ_p	ε	qR
XL52, R=200 nm σ=9%, τ_b=0.0193 s	0.60	0.637	0.217	2.01, 2.93, 3.57, 4.15
XL63, R=185 nm σ=8%, τ_b=0.0153 s	0.563	0.595	0.142	1.86, 2.71, 3.30, 3.84
	0.574	0.606	0.164	3.30
	0.584	0.616	0.185	2.71, 3.30, 3.84
	0.600	0.631	0.217	1.86, 2.71, 3.30, 3.84

spheres, its aging was exposed.[14] However, at that time, the process was neither quantified nor analyzed in detail.

A preliminary quantitative account of aging of the glass of hard sphere colloids was presented in a recent Letter.[15] This paper presents not only a more extensive examination of the processes but also details, in Sec. II, the protocols used to acquire good estimates of ensemble averages for processes whose decay times exceed any practical measurement time, as well as methods for distinguishing between reversible and irreversible (aging) processes, however slow or fast each of these may be. In Sec. III, results are presented and discussed for several volume fractions, and a range of wavevectors around the main peak of the static structure factor. Conclusions are presented in Sec. IV.

II. METHODS

A. Sample description

The particles used in these experiments comprise cores of a copolymer of methylmethacrylate and trifluoroethyl acrylate with coatings of poly(12-hydroxystearic acid) approximately 10 nm thick.[16] Average hydrodynamic radii, R, and polydispersities, σ, listed in Table I, were determined by DLS and static light scattering on very dilute samples.[17] Suspension of the particles in *cis*-decalin achieves matching of the refractive indices of particulate and suspending phases to a degree that effectively suppresses multiple scattering over the range of scattering vectors (between qR$\approx$1.5 and qR$\approx$4) spanned in these experiments. The reduction in van der Waals attraction this matching achieves, along with the lack of detectable charge on the particles, means that the interactions between them are dominated by the short range repulsion effected by the solvated surface coatings.[18] Hence these suspensions present a good approximation to the perfect hard sphere system. Accordingly, after mapping the equilibrium phase behavior observed for these suspensions onto that known for the perfect, one-component hard sphere system, the volume fractions ϕ_f=0.493 and $\phi_m\approx$0.54 of coexisting fluid and crystal phases can be identified.[5] With this reference, the observed glass transition is located at $\phi_g\approx$0.57.[6]

Alternatively, using the results of recent computer simulations, one can employ, in the above manner, the freezing volume fraction $\phi_f(\sigma)$ of a system of hard spheres with a finite spread σ in the particle size distribution (PSD). From Ref. 19 one reads, for example, $\phi_f(8\%)\approx$0.527. It has been argued that a comparison between different systems requires the volume fraction to be referenced in this way.[20] However, the available computational data for $\phi_f(\sigma)$ is limited to symmetrical PSDs, while those of the type of polymer particles used here tend to be negatively skewed.[17] So, rather than introducing ambiguity due to the influence of the shape of the PSD by attempting to express the volume fraction in absolute terms, and to remain consistent with the vast majority of literature, the stated sample volume fractions will be read here relative to the freezing value, ϕ_f=0.493. For comparison, however, volume fractions relative to the freezing point for a symmetrical PSD are provided in Table I. Alternatively, the thermodynamic phase point may be expressed in terms of the degree of undercooling or overpacking in this case, $\varepsilon=(\phi/\phi_f-1)$. Two different latex suspensions are used in this work. Their radii and polydispersities, as well as volume fractions and scattering vectors studied are given in Table I. Despite the slight differences between the two lattices, the DLS results are consistent.

Prior to the start of a measurement, each sample was tumbled for at least 24 h. The DLS results were found to be independent of the tumbling time, although even brief tumbling effectively shear melts any colloidal crystals that may be present. The waiting time origin, t_w=0, is the time a sample was placed in the spectrometer immediately after tumbling was stopped. In the results below delay times, τ, are expressed in units of the Brownian time, $\tau_B=R^2/(6D_o)$, where D_o is the diffusion constant for freely diffusing particles (Table I). Waiting times, t_w, are expressed in hours.

B. Light scattering procedures

The quantity of interest, and that from which other dynamical properties are derived in this paper, is the intermediate scattering function or autocorrelation function of the qth spatial Fourier component $\rho(q,\tau)$ of the particle number density fluctuations,

$$f(q,\tau)=\langle\rho(q,0)\rho^*(q,\tau)\rangle/\langle|\rho(q)|^2\rangle, \quad (1)$$

where the asterisk denotes the complex conjugation.

For the purpose of justifying the protocols adopted, we show in Fig. 1, a typical result for the ISF, $f(q,\tau)$, for several waiting times, t_w. One sees first that $f(q,\tau)$ fails to decay to zero in the experimental time window and second, that $f(q,\tau)$ varies with waiting time, t_w. Respectively, these indicate nonergodicity and nonstationarity—features of the glass and complications for the experimentalist not normally associated with the fluid state. One also notes that a plateau separates an initial (fast) decay from a slow decay that stretches out as t_w increases. Whether the fast process is independent of t_w, as it appears to be, is one of the aspects of the relaxation dynamics examined below.

As proposed elsewhere,[15] the stretching function

$$n(q,\tau)=\frac{d\log(w(q,\tau))}{d\log\tau}, \quad (2)$$

where

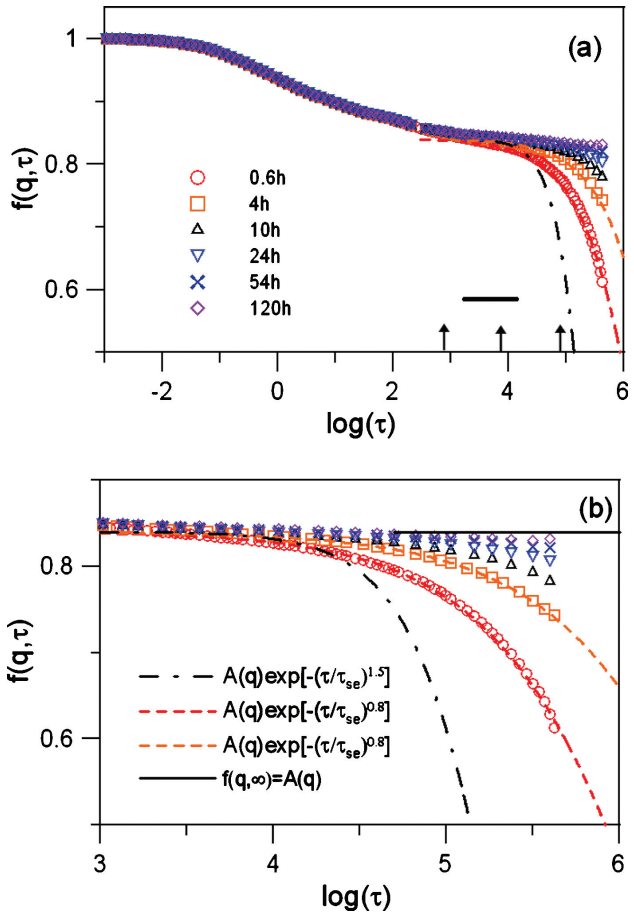

FIG. 1. ISF vs logarithm of delay time for qR=2.93 and ϕ=0.60 at waiting times indicated. Arrows in (a) indicate measurement times, T_1/τ_b, and the small horizontal bar indicates the range of variation in crossover time, $\tau_m(q)$, with waiting time (see text for details). (b) Expanded scale of delay time highlights quality of stretched exponentials fits; values of τ_{se} are (left to right) 2.2×10^5, 2.1×10^6, and 6.5×10^6.

$$w(q,\tau) = -q^2 \ln f(q,\tau) \tag{3}$$

is an alternative presentation of the data. One sees from examples shown in Fig. 2 that their minima, $\nu(q) = \min[n(q,\tau)]$, deepen and shift to longer delay times, $\tau_m(q)$, as the sample ages. We identify $\tau_m(q)$ as the crossover time from the fast process to the slow process. It is also the delay time where the non-Fickian, or collective, dynamics are most strongly exposed. Accordingly we give considerable currency to the quantities $\tau_m(q)$, $\nu(\tau_m(q))$, and $f(q,\tau_m(q))$.

One way to deal with nonergodicity is with the approach introduced by Pusey and van Megen.[7,21] This assumes that the space-time density fluctuations can be decomposed into an arrested, time-invariant component and a time dependent, fluctuating component. The resulting scattered light field comprises constant and fluctuating components. Stationarity is implicit. Then, provided the spatial correlation of both components is much smaller than the linear dimension of the scattering volume, thereby allowing the central limit theorem to be effected, the fluctuating field is a complex, Gaussian variable of zero mean. These considerations lead to the following expression for the ISF (Ref. 7):

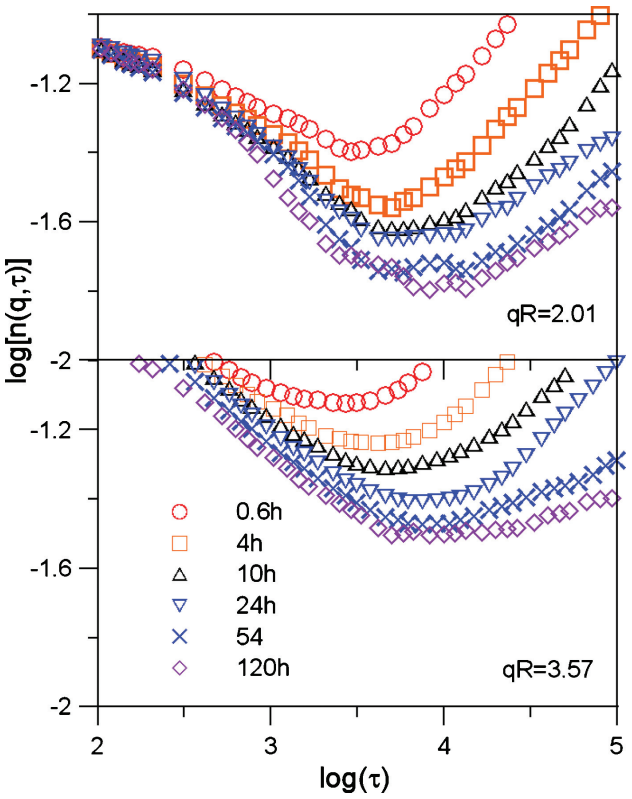

FIG. 2. Double logarithm plots of the stretching functions [Eqs. (2) and (3)] for ϕ=0.60 vs delay time for wavevectors and waiting times indicated.

$$f_1(q,\tau) = 1 + \frac{\langle I\rangle_{T_1}}{\langle I\rangle_E}\left\{\left[\frac{\langle I(q,0)I(q,\tau)\rangle_{T_1} - \langle I^2(q)\rangle_{T_1}}{\langle I(q)\rangle^2_{T_1}} + 1\right]^{1/2} - 1\right\}. \tag{4}$$

The brackets, $\langle\cdots\rangle_{T_1}$, express the time average over the intensity fluctuations, I(q,t), of a single speckle (or spatial Fourier component of the particle number density fluctuations) accumulated in a single measurement of duration T_1, and $\langle\cdots\rangle_E$ express the ensemble average, acquired by averaging over a large number ($\approx$4000) of speckles, achieved here in a single rotation of the sample. The nonergodicity factor, or Debye–Waller factor in this case, $f_1(q,\infty)$, follows from Eq. (4) in the limit $\tau\to\infty$,

$$f_1(q,\infty) = f_1(q,\tau) \to \infty = 1 + \frac{\langle I(q)\rangle_{T_1}}{\langle I(q)\rangle_E}\left\{\left[2 - \frac{\langle I^2(q)\rangle_{T_1}}{\langle I(q)\rangle^2_{T_1}}\right]^{1/2} - 1\right\}. \tag{5}$$

The derivation of Eq. (4) assumes a detector area smaller than one coherence area, i.e., only a single spatial Fourier component of the scattered light is detected. The subscript "1" is used to denote results obtained by the above procedure.

Another approach is to accumulate the time averages of the intensities, $\langle I(q)\rangle^{(i)}_{T_2}$, and intensity autocorrelation functions (ACFs), $\langle I(q,0)I(q,\tau)\rangle^{(i)}_{T_2}$ for a (large) number M of independent spatial Fourier components of the particle num-

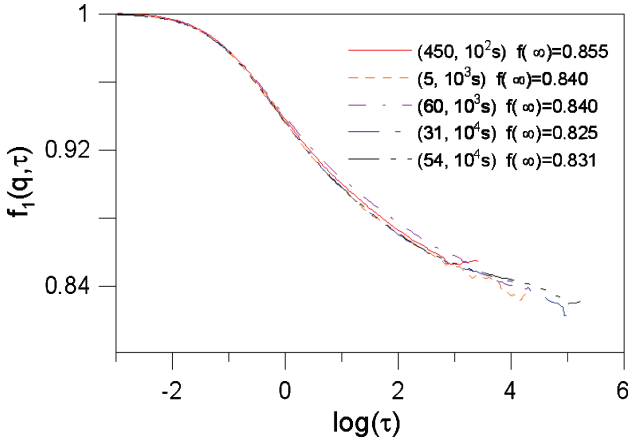

FIG. 3. ISF from PvM method vs logarithm of delay time at qR=2.93 for ϕ=0.60 for several values of the number of measurements (n) and duration (T_1), as indicated in parentheses (n, T_1). Note the expanded vertical scale.

ber density fluctuations. From these one estimates the (normalized) ensemble-averaged intensity ACF as follows:

$$g_E(q,\tau) = \frac{\frac{1}{M}\Sigma_i \langle I(q,0)I(q,\tau)\rangle_{T_2}^{(i)}}{\left[\frac{1}{M}\Sigma_i \langle I(q)\rangle_{T_2}^{(i)}\right]^2}. \quad (6)$$

In some of the earliest studies of colloidal glasses,[6,9] the "brute force" accumulation implied by Eq. (6) was achieved rather inefficiently by either translation or rotation of the sample between individual measurements. Aging was neither observed nor considered. An accumulation of independent spatial Fourier components of the fluctuations, efficient enough to resolve nonstationary processes, can now be achieved by either collecting images of the far field intensity distribution (or speckle pattern) on a charge coupled device (CCD) camera,[22] or by gating the intensity of the scattered light collected by a standard photomultiplier tube, while the sample is rotated continuously.[13,23] Either procedure provides an average over some 4000 speckles. Technicalities place lower limits on the respective delay time windows of order

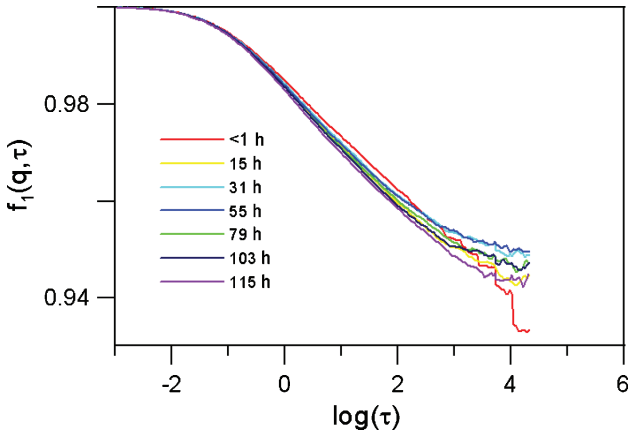

FIG. 4. ISF from PvM method vs logarithm of delay time for several waiting times (qR=3.57 and ϕ=0.60). Each curve presents an average over ten measurements with duration of 1000 s. Note that the value of qR and the scale of the ordinate differ from Fig. 3. Note the expanded vertical scale.

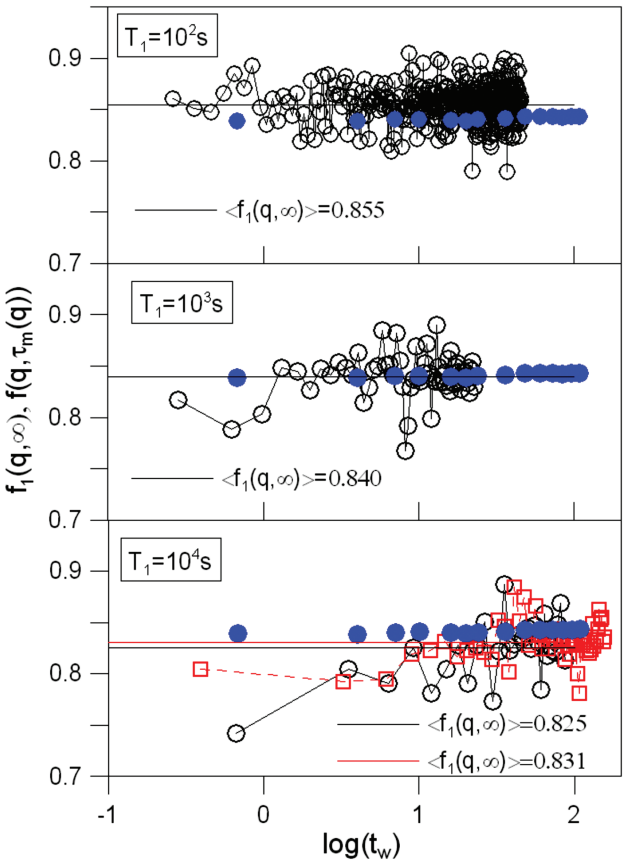

FIG. 5. Nonergodicity factor $f_1(q,\infty)$ [Eq. (5)] vs logarithm of the waiting time (hours), shown by open circles and squares, for measurement times, T_1, indicated (qR=2.93 and ϕ=0.60). Open circles and squares seen in the bottom panel derive from independent sets of measurements. Values of these nonergodicity factors averaged over all waiting times are given and shown by horizontal lines. The ISF $f(q,\tau_m(q))$ at the crossover are shown by the filled circles.

of 0.1 and 1 s, and this limitation necessitates complementary measurement of faster processes by the Pusey and van Megen (PvM) method.

Of the two procedures based on continuous rotation, interleaved sampling[13] and the method of echoes,[23] the second is employed here. It has the higher resolution and is able to account for errors in the period of rotation. Presuming the 4000 or so speckles accumulated in a single rotation provides the basis for an adequate estimate of the ensemble averaged intensity ACF, Eq. (6), the ISF can be calculated with the usual factorization property of a zero mean, complex Gaussian light field,[7]

$$g_E(q,\tau;t_w) = 1 + c|f_2(q,\tau;t_w)|^2. \quad (7)$$

Explicit dependence on the waiting time, t_w, is denoted here in the expectation that the slower processes, at least, may be nonstationary.

The unknown experimental factor c, in Eq. (7), is fixed by requiring that the results of the two measurements match, i.e., $|f_1(q,\tau)|^2=|f_2(q,\tau;t_w)|^2$, for that range of delay times (around 1 s), where the results of the two procedures overlap. So the normalization of $f_2(q,\tau;t_w)$ depends on $f_1(q,\tau)$. The subscript 1 or 2 is then dropped from the final ISF so obtained.

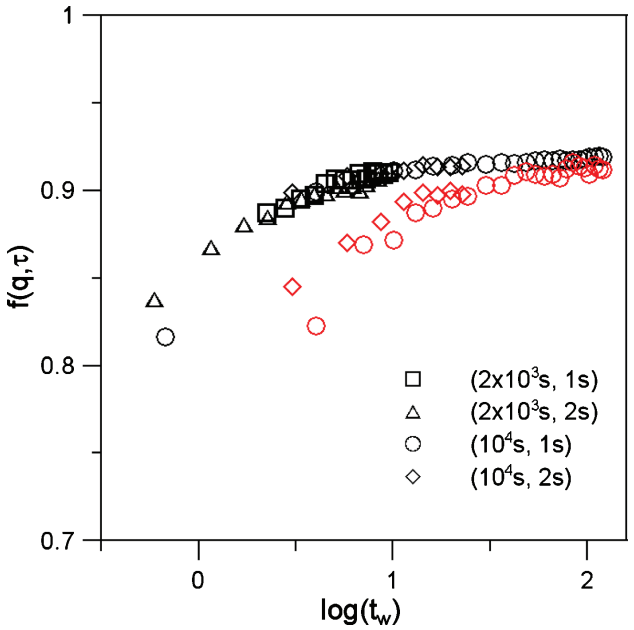

FIG. 6. ISF, $f(q,\tau)$ vs logarithm of the waiting time at delay times $\tau=8\times10^4$ (upper data set) and $\tau=4\times10^5$ (lower data set). Measurement time T_2 and rotation period t_r are indicated in parentheses (T_2,t_r).

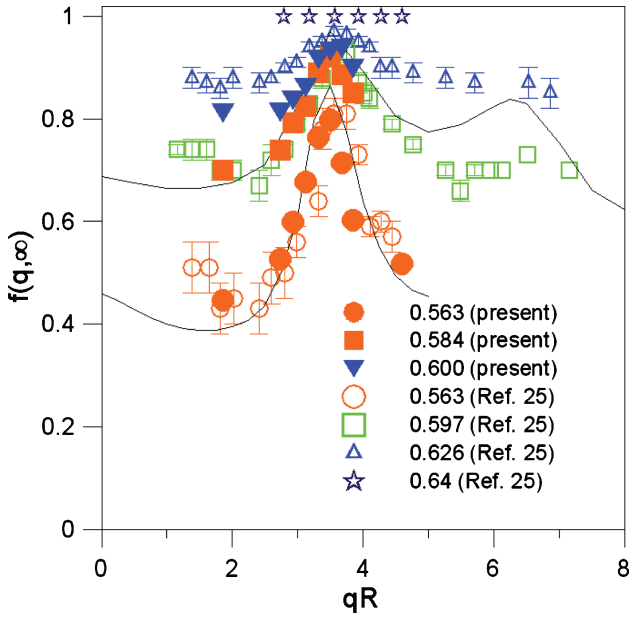

FIG. 8. Nonergodicity factors $f(q,\infty)$ vs wavevector for volume fractions indicated. Solid symbols are the present data and the open symbols are results from Ref. 25. The solid lines are from MCT (Ref. 8).

The duration T_1 of the measurement of the ISF by the PvM method was selected so as to maximize inclusion of the fast, and predominantly stationary processes and minimize the inclusion of slow, nonstationary processes. Thus, the upper limit of the time window of this part of the measurement must be at least comparable to $\tau_m(q)$. The duration T_2 (2000–10 000 s) of individual measurements by the echo method was selected to best expose nonstationary processes.

Figure 3 shows $f_1(q,\tau)$ for values of T_1 of 100, 1000, and 10 000 s. The upper limits of the time windows, T_1/τ_b, corresponding to these values of T_1 are indicated in Fig. 1.

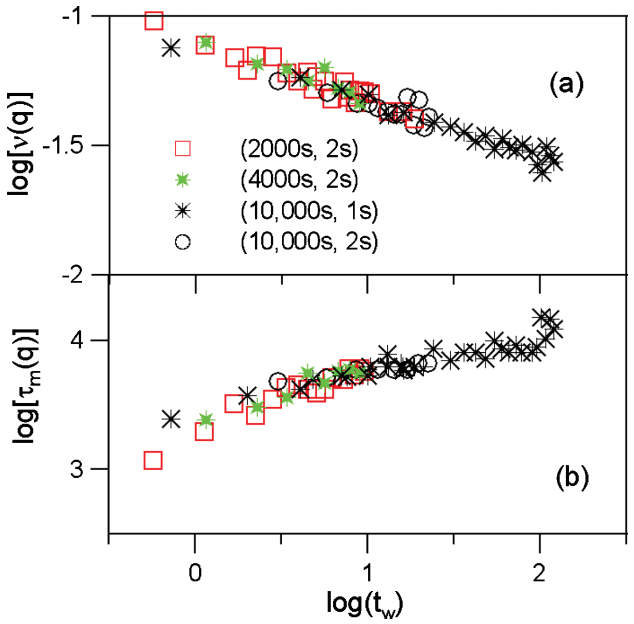

FIG. 7. Double logarithm plots of (a) stretching index $\nu(q)$ and (b) crossover time $\tau_m(q)$ vs waiting time. Measurement time T_2 and rotation period t_r are indicated in parentheses (T_2,t_r).

Figure 4 shows $f_1(q,\tau)$ for values of t_w, from 1 to 115 h. These two figures indicate that any effects that the measurement time and waiting time may have on the ISF, measured by the PvM approach, are within experimental noise. However, a subtlety is exposed in Fig. 5, where the nonergodicity factors, $f_1(q,\infty)$, obtained by Eq. (5), are shown as functions of t_w for the above values of T_1. As is evident from Eq. (5), the greater the spread, $\langle I^2(q)\rangle_{T_1}$, of intensity fluctuations accumulated in the given measurement, irrespective of whether these derive from stationary or nonstationary processes, the smaller the corresponding value of $f_1(q,\infty)$. So, one sees that increasing T_1 from 100 s to 10 000 s results in a decrease of some 3% in the average nonergodicity factors, $f_1(q,\infty)$.

This small variation with T_1 is effectively washed out when the results obtained by the PvM and echo methods are averaged in the time window where they overlap. The final ISF, $f(q,\tau;t_w)$, is insensitive to variation of T_1 from 100 to 10 000 s. In particular, $f(q,\tau_m(q))$, the ISF at the crossover is independent of T_1 and, as may be seen in Fig. 5, shows no variation with t_w. Accordingly, the measurement time T_1 (=1000 s in this case) selected is that for which $\langle f_1(q,\infty)\rangle = f(q,\tau_m(q))$; i.e., the conditions for which the nonergodicity factor coincides with the ISF at the crossover. This criterion removes the ambiguity, although a small one, from our experimental definition of the nonergodicity factor. The latter is henceforth denoted without subscript as $f(q,\infty)$. Of course for a given set of conditions preliminary measurements must be made in order to estimate $\tau_m(q)$ and $f(q,\tau_m(q))$ approximately before determining the final protocol.

Finally, we demonstrate that the rotation of the sample does not influence the dynamics. Figure 6 illustrates that $f(q,\tau)$, shown for two delay times, is not affected by either the rotation period or the time, T_2, for which the sample is rotated and the measurement performed. Figures 7(a) and 7(b) show that the parameters $\nu(q)$ and $\tau_m(q)$ are also unaf-

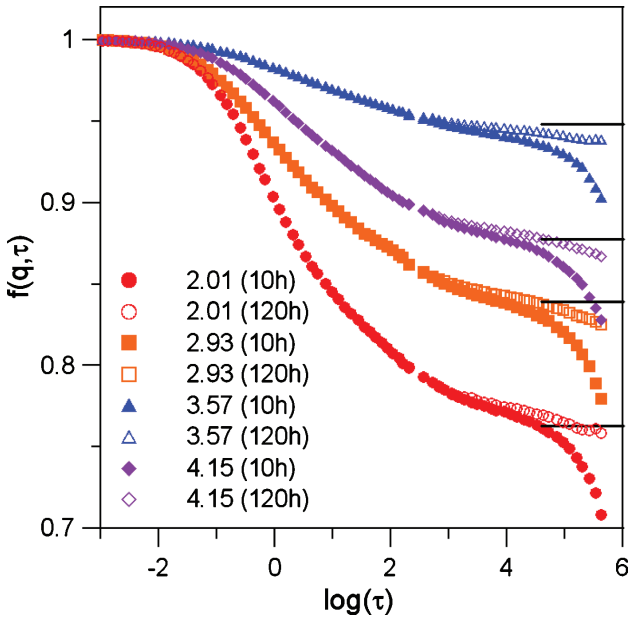

FIG. 9. The ISF vs logarithm of delay time for $\phi=0.580$ for wavectors and waiting times indicated in parentheses. For each case, the nonergodicity parameter $f(q,\infty)$ is indicated by a horizontal line.

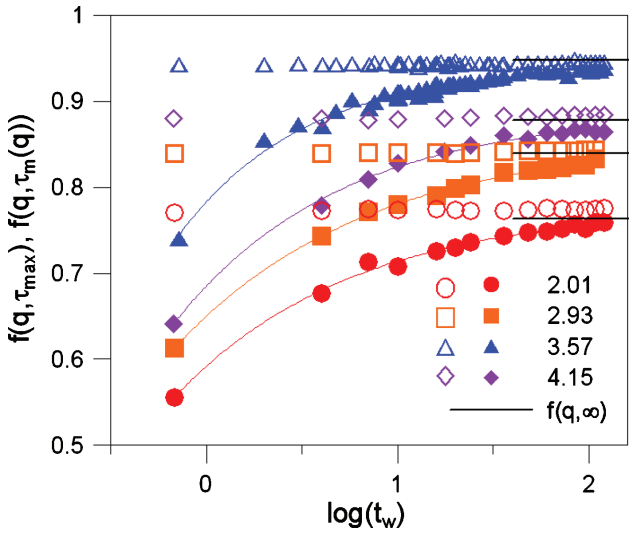

FIG. 10. $f(q,\tau_{max}\approx 4.5\times 10^5)$ (filled symbols) and $f(q,\tau=10^4\approx\tau_m(q))$ (open symbols) as functions of the waiting time for several values of qR indicated. Lines are fits of Eq. (8) to the data. Values of $f(q,\infty)$ are indicated by small horizontal lines.

fected by these times. It is appropriate here to mention that a recent study[24] of aging of a water-oil emulsion shows consistency of results obtained by imaging the speckle pattern on a CCD (i.e., without rotation of the sample) and the method of echoes (with rotation).

III. RESULTS AND DISCUSSION

A. Aging of a colloidal glass

The main result from the previous section is that the nonergodicity factor, $f(q,\infty)$, is a stationary property of the colloidal glass investigated here, at least for the wavevectors (listed in Table I) around the position, given by $qR\approx 3.6$, of the main peak of the static structure factor. Values of $f(q,\infty)$ obtained in this work are shown in Fig. 8. They are consistent with those of previous studies[25] and MCT.[8]

Figure 9 shows the ISFs for several wavevectors. As in Fig. 1, aging is most pronounced at the upper limit $\tau_{max}=4.5\times 10^5$ of the time window but imperceptible at the crossover. We quantify the aging process by plotting, as in Fig. 10, the ISF as a function of the waiting time, for fixed values of the delay time. The power law,

$$f(q,\tau;t_w)=A(q)\left[1-\left(\frac{t_w}{t_0}\right)^{-b}\right], \tag{8}$$

is the simplest function with which we can describe the variation in the decay of the ISF with t_w. Fitting this to the ISFs for the range of delay times from the crossover time, τ_m ($\sim 10^4$), to τ_{max} consistently gives the same values for A(q), as seen in Fig. 11(a). From the latter, one also sees within experimental uncertainty that A(q) coincides with the nonergodicity factor, $f(q,\infty)$, and therefore with the ISF, $f(q,\tau_m(q))$ at the crossover. Thus, following the tumbling, an action one might consider as synonymous with a quench, the perfect "aged" glass, that for which the ISF decays to a constant value, say $f(q,\tau>\tau_m(q))=f(q,\infty)=A(q)$, is approached algebraically with waiting time. The other two parameters, b and t_o, in Eq. (8) are shown in Figs. 11(b) and 11(c). As indicated, uncertainties are appreciable and any dependence

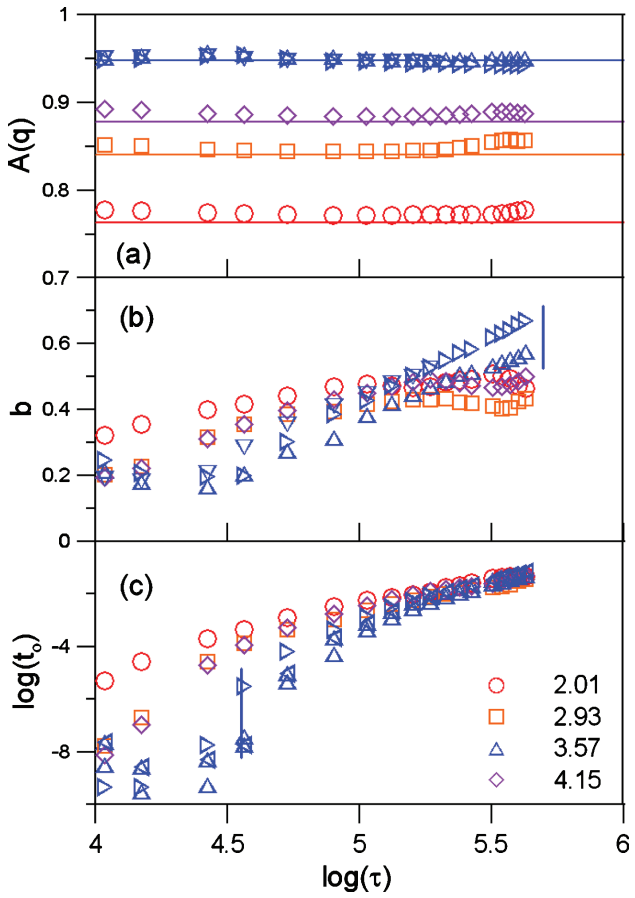

FIG. 11. Parameters A(q), b, and t_o of the power law, Eq. (8) vs logarithm of delay time for values of qR indicated. Lines are $f(q,\infty)$. For $qR=3.57$ results of several independent experiments are indicated by triangles in different orientations. Vertical bars are indicative of experimental uncertainty.

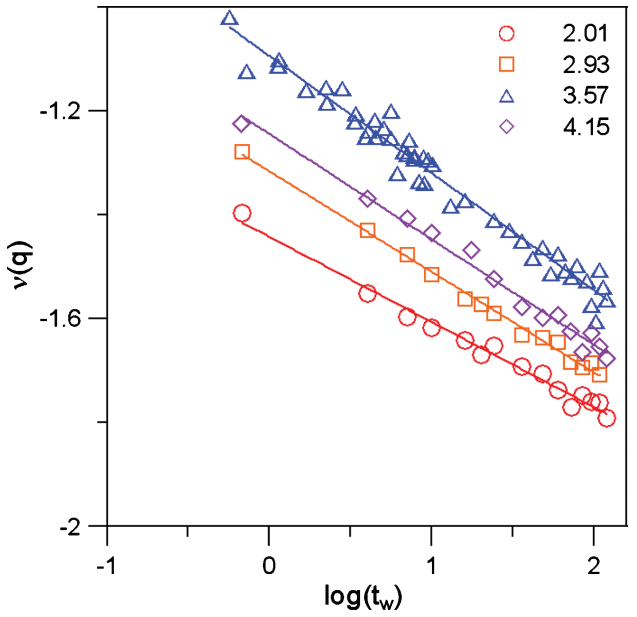

FIG. 12. Double logarithm plots of the stretching index $\nu(q)$ vs waiting time t_w for values of qR indicated. Lines are power laws, Eq. (9), fitted to the data. The fitting parameters ζ and ν_o are given in Table II.

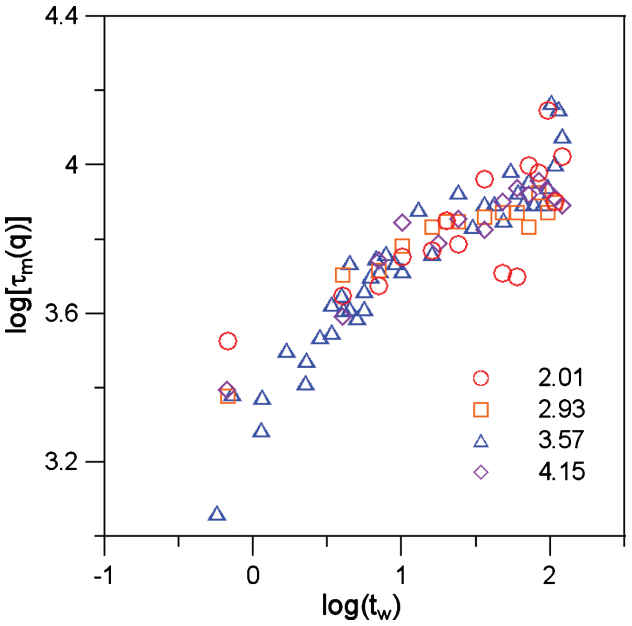

FIG. 13. Double logarithm plot of delay time $\tau_m(q)$ at the crossover from fast to slow processes vs waiting time t_w at indicated values of qR.

these quantities may have on the wavevector cannot be discerned with confidence. These results are, however, not inconsistent with the expectation that as the delay time is increased a larger amplitude, t_o^b, of the nonstationary processes is obtained.

From Fig. 1 and the discussion in Sec. II B, it would appear that the ISF can be neatly and conveniently divided into a fast, stationary component and a slow, nonstationary component. We investigate the crossover between these components more closely, first, with the stretching index, which is identified as the minimum in the stretching function [Eq. (2)]: $\nu(q)=\min[n(q,\tau)]$. Were the fast processes [i.e., processes in the window $\tau<\tau_m(q)$] strictly stationary and, thereby, decoupled from the slow nonstationary processes, one would expect $\nu(q)$ to be independent of t_w. Accordingly, the waiting time dependence of $\nu(q)$, shown in Fig. 12, exposes a coupling, however weak, between the fast and slow processes. Moreover, as illustrated, this coupling decreases algebraically with waiting time,

$$\nu(q) = \nu_o t_w^{-\zeta}. \tag{9}$$

Second, the variation of the crossover time $\tau_m(q)$ with t_w is shown in Fig. 13. So, the stationarity found for the amplitude, $f(q,\tau_m(q))$ above, is not replicated by the other quantities, $\nu(q)$ and $\tau_m(q)$, that characterize the crossover from fast to slow processes. However, in view of the noise on these data, the possibility that $\tau_m(q)$ ultimately approaches a constant value cannot be excluded. Note also that $\tau_m(q)$ shows no systematic dependence on the scattering vector.

We digress to point out that this scale invariance of $\tau_m(q)$ is seen only in the glass and not generally for colloidal fluids. Around the freezing value, $\phi\approx\phi_f$, $\tau_m(q)$ varies by approximately a factor of 10 over the range of q values considered here. This q-dependence of $\tau_m(q)$ gradually disappears as ϕ approaches ϕ_g.[12]

One sees from Table II that this apparent lack of sensitivity to the spatial scale, q, also applies to the exponent, ζ, but not to the amplitude, ν_o [Eq. (9)]. So, the latter appears to be the only quantity which characterizes aging of the crossover from fast to slow processes that shows any significant dependence on q. The (normalized) ratios $\nu_o/f(q,\infty)$ and $\nu_o/S(q)$ are also listed in Table II. Despite the appreciable uncertainty in these ratios, they show that the q-dependence of ν_o is in much closer harmony with $f(q,\infty)$ than with S(q). So, if there is a correlation of the aging dynamics with the structure then it is more likely to be with the arrested structure, expressed by $f(q,\infty)$, than with the total structure, expressed by S(q).

TABLE II. Values of the fitting parameters ν_o and ζ for the waiting time dependence of the stretching index [Eq. (9)] for XL52 at $\phi=0.60$. The values in the fourth and fifth columns are normalized to unity at qR=3.57. The structure factor S(q) has been calculated by the Percus–Yevick approximation for hard spheres having polydispersity of 8% (Ref. 26).

qR	Amplitude ν_o ±0.001	Aging exponent ζ ±0.02	$\nu_o/f(q,\infty)$	$\nu_o/S(q)$	S(q) ϕ=0.6
2.01	0.037	0.18	0.6	60	0.022
2.93	0.049	0.20	0.7	11	0.150
3.57	0.080	0.22	1.0	1.0	3.11
4.15	0.056	0.20	0.7	4	1.38

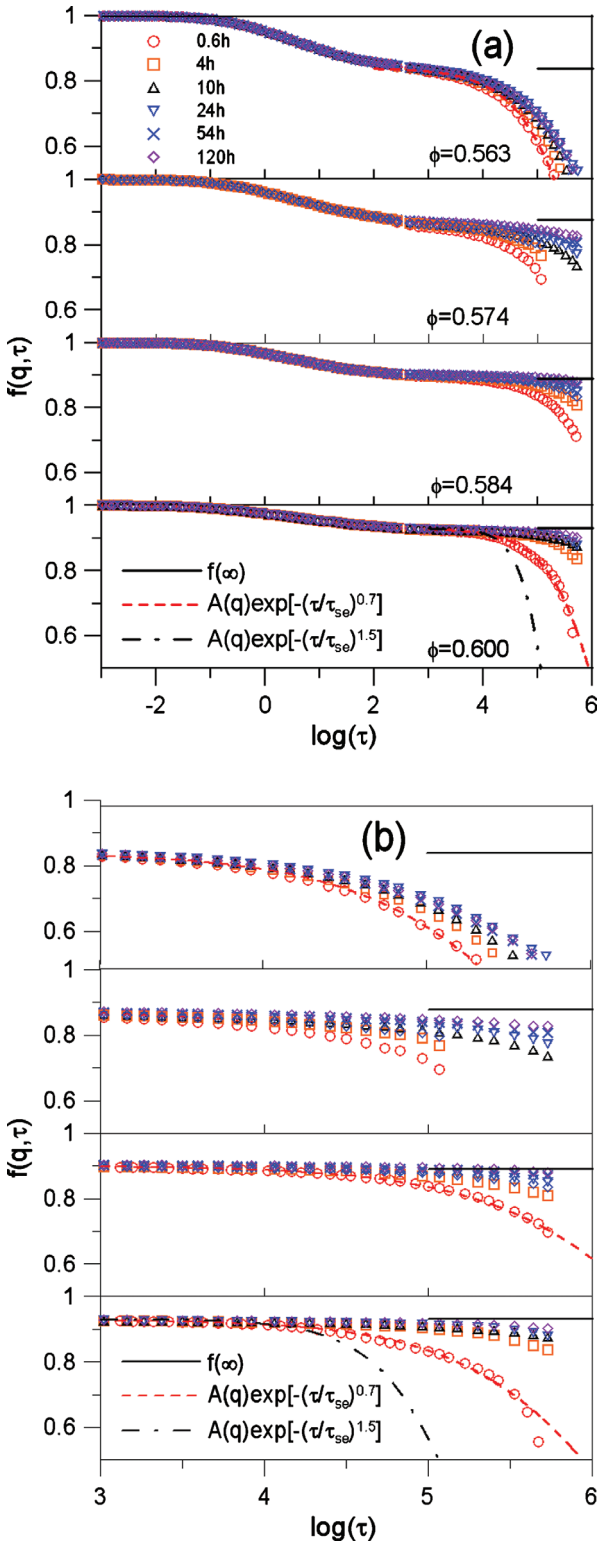

FIG. 14. ISF vs logarithm of delay time, at qR=3.30 for waiting times and volume fractions indicated. (b) Expanded scale of delay time giving clearer fits to stretched exponentials.

Finally, we quantify the slow decays of the ISF (Fig. 1) in terms of the generalized exponential,

$$f(q,\tau > \tau_m(q)) = A(q)\exp[-(\tau/\tau_s)^{\delta}]. \quad (10)$$

We use the values for A(q) obtained above, leaving τ_s and δ as fitting parameters. The fits and fitting parameters are

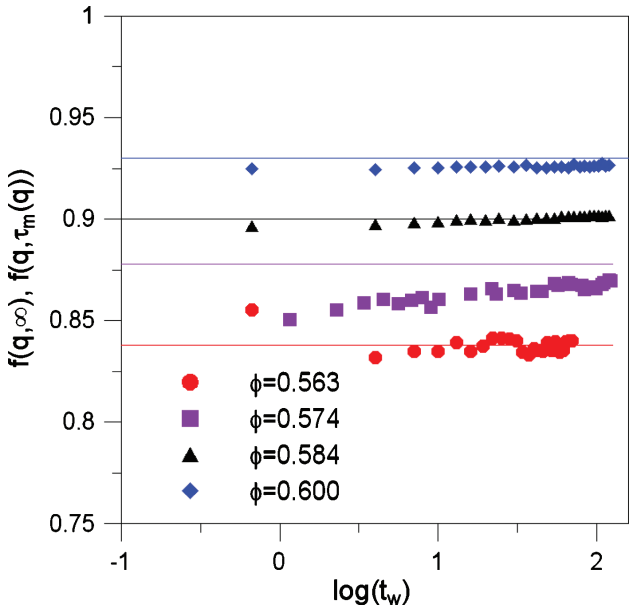

FIG. 15. The ISF $f(q,\tau_m(q))$ at the crossover vs logarithm of the waiting time (hours) for volume fractions indicated (qR=3.30). The horizontal lines indicate the (average) nonergodicity factors $f(q,\infty)$.

shown in Fig. 1. Although this analysis is limited for the present data by the limited decays of the ISFs from their respective plateaux, it is quite clear that $\delta<1$, i.e., the time correlation function of the nonstationary processes follow a stretched exponential function of the delay time. So, whatever the nature of the aging dynamics in these colloidal glasses, it differs in some basic respect from aging characterized by compressed exponential decays with $\delta\approx1.5$, found in other complex, arrested materials mentioned in Sec. I. However, due to the limited extent of the decays from the

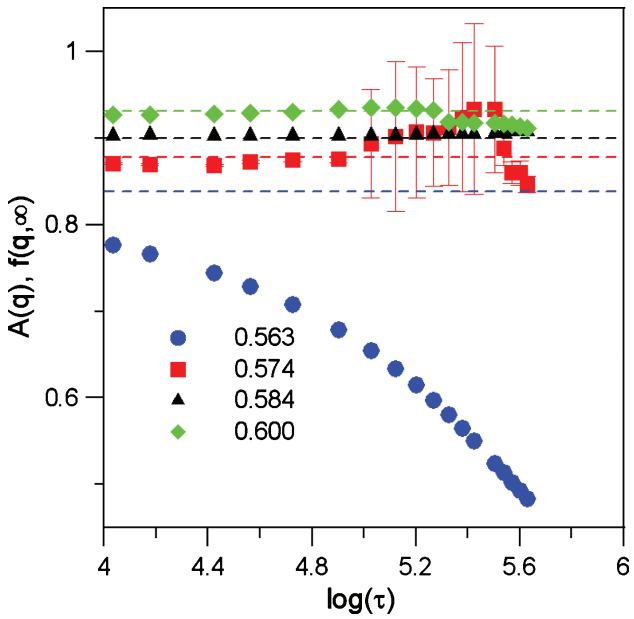

FIG. 16. Parameters, A(q) of the power law, Eq. (8) vs logarithm of delay time, for volume fractions indicated (qR=3.30). Dashed lines are the nonergodicity factors, $f(q,\infty)$. The large errors for ϕ=0.574 result from the shorter measurement time T_2 of 2000 s in this case for smallest waiting times (note also corresponding maximum delay times in the second panel of Fig. 14).

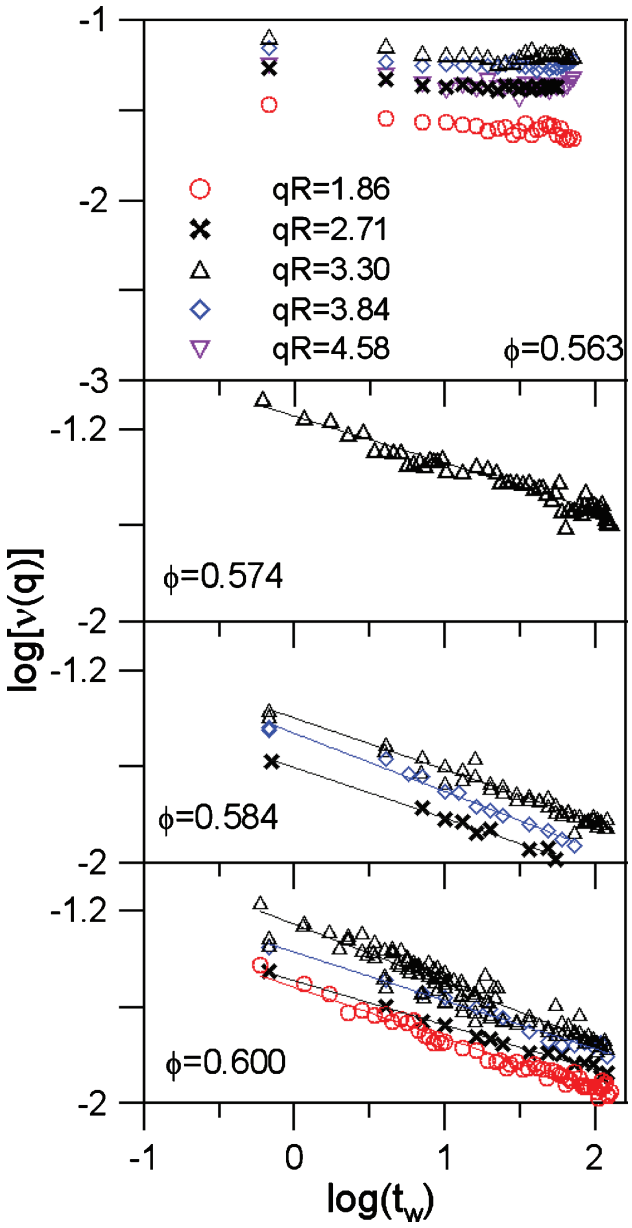

FIG. 17. Double logarithm plots of stretching index vs waiting time t_w for values of qR and volume fractions indicated. Lines are power laws, Eq. (9), fitted to the data. Values of the fitting parameters ζ and ν_o are given in Table III.

plateaux there is insufficient information to quantify the q-dependence of τ_s or for that matter, to preclude the possibility of a crossover to a power-law as observed in computer simulations of molecular glasses.[3,4]

B. Effect of volume fraction

The results presented in this subsection are based on measurements with samples denoted as XL63 in Table I. Figure 14 shows the ISFs obtained by the procedures described in Sec. II B for several volume fractions. The results are qualitatively similar to those in Figs. 1 and 9. Again, the age dependent decays from the respective plateaux can be described by stretched exponential functions of delay time. As illustrated in Fig. 15 for several volume fractions, the ISF at the crossover, $f(q,\tau_m(q))$, coincides, within experimental noise, with the nonergodicity factor, $f(q,\infty)$.

Except for the lowest volume fraction, the manner by which the ISFs, $f(q,\tau>\tau_m(q);t_w)$, age can be described by the power law, Eq. (8). Moreover, as found for the colloidal glass in Sec. III A, the amplitude A(q) of the power law agrees with the nonergodocity factor, $f(q,\infty)$ (see Fig. 16). The slow decay of the ISF for the sample at the lowest volume fraction studied, $\phi=0.563$ ($\approx\phi_g$), shows only limited dependence on t_w. Once this exceeds some 10 h stationarity appears to be attained (see top panels in Fig. 14(a) and 14(b)). The ISFs for suspensions at lower volume fractions ($\phi<\phi_g$) show no dependence on t_w (data not shown). So, as proposed in the previous work,[12] around ϕ_g there is a change from reversible to irreversible in the processes that effect the final decay of the ISF. This identification of the operational GT is independent of the experimental time window provided, of course, its upper limit exceeds the crossover, $\tau_m(q)$, by a margin sufficient to observe some decay from the plateau. Increasing the time window beyond the present τ_{max} would coarse grain over the very nonstationary processes we are attempting to resolve.

The stretching indices, $\nu(q)$, are shown as functions of the waiting time in Fig. 17. For $\phi=0.563$ these show only a weak decrease with waiting time beyond experimental noise. For the remaining cases the waiting time dependence of $\nu(q)$ can be described by the power law given by Eq. (9). As found in Sec. III A for the glass of XL52, the exponents ζ (see Table III) for the highest two volume fractions show no systematic dependence on wavevector. Moreover, they do not exhibit a detectable dependence on volume fraction. Also as found in Sec. III A, the variations of the amplitudes, ν_o, with q are in closer harmony with $f(q,\infty)$ than they are with S(q).

TABLE III. Values of the fitting parameters for the waiting time dependence of the stretching index [Eq. (9)] for two volume fractions of XL63. For $\phi=0.574$, data was only collected at qR=3.30, which yielded $\nu_o=0.072$ and $\zeta=0.20$. See Table II for definitions.

	$\phi=0.584$			$\phi=0.600$		
qR	Amplitude ν_o	Aging exponent ζ	S(q)	Amplitude ν_o	Aging exponent ζ	S(q)
1.86	⋯	⋯	⋯	0.030	0.21	0.018
2.71	0.025	0.21	0.10	0.032	0.19	0.08
3.30	0.040	0.21	0.90	0.056	0.23	0.70
3.84	0.035	0.23	2.56	0.043	0.20	2.94

IV. CONCLUSIONS

In the above, we have reported the results of DLS measurements of the coherent ISF of glasses of colloidal hard spheres for several volume fractions and scattering vectors bracketing the primary peak of the static structure factor. The main results are summarized as follows:

(1) In all cases the ISF features a clear crossover at delay time $\tau_m(q)$ from an initial, predominantly stationary decay to a slower nonstationary decay.
(2) The ISF at the crossover $f(q,\tau_m(q))$ coincides with the (independently measured) Debye–Waller factor, $f(q,\infty)$.
(3) Slow, nonstationary decays, i.e., $f(q,\tau>\tau_m(q);t_w)$, insofar as they can be quantified in this work, follow stretched exponential functions of delay time.
(4) The deviation from the perfect aged glass, $f(q,\tau>\tau_m(q)t_w)$-$f(q,\infty)$, decreases with waiting time in a power-law fashion, i.e., stationarity is approached algebraically.

In addition to these direct observations of the aging process itself, the delay time $\tau_m(q)$, the degree of stretching $\nu(q)$, and the value $f(q,\tau_m(q))$ of the ISF at the crossover are perhaps more significant in that their analysis, by exposing a coupling of aging to the fastest processes detected in these experiments, hints at the more fundamental mechanisms that drive aging.

So, while on the face of it, the initial fast decay $f(q,\tau<\tau_m(q))$ of the ISF exhibits no dependence on the waiting time t_w, i.e., it appears to be stationary, it cannot be strictly so because the index, $\nu(q)$, a quantity indicative of the coupling between the fast and the slow, nonstationary processes, is finite and age dependent. Only for the perfect glass, an idealization approached algebraically with t_w, are all processes stationary. Conversely, one infers that $\nu(q)$ is a measure of those nonstationary, ergodicity restoring processes absent in the perfect glass. So, it comes as no surprise that the manner in which the amplitude, ν_o of the power law [Eq. (9)] that characterizes the aging of $\nu(q)$, varies with scattering vector follows the amplitude of the arrested structure, $f(q,\infty)$, rather than that of the total, average structure, $S(q)$.

As far as we can gauge from the range of parameters covered in these experiments, the exponent, ζ, of the power law just mentioned, shows no significant dependence on either scattering vector or volume fraction. Also the crossover time, $\tau_m(q)$, shows no variation with scattering vector. This observation should be seen in the context of a previous study[12] of the metastable fluidlike states of these suspensions ($\phi_f<\phi<\phi_g$). It was found that the q-dependence of $\tau_m(q)$ varies approximately in harmony with $S(q)$ around ϕ_f, but that this q-dependence disappears as ϕ_g is approached. So as the GT is approached and density fluctuations become arrested, the irreversible processes that emerge posses a degree of spatial scale invariance. This, along with the algebraic dependence of the index, $\nu(q)$, and the difference, $f(q,\tau>\tau_m(q))$-$f(q,\infty)$, on waiting time indicate that aging is an intermittent rather than a continuous process.

Ultimately and however slowly, and provided the particles' sedimentation velocities and polydispersity are not too large, these colloidal glasses crystallize.[5,27,28] The mechanism by which they do so appears to be qualitatively different from that, via homogeneous nucleation, seen for crystallization in metastable colloidal fluids ($\phi_f<\phi<\phi_g$).[20,27] However, whatever the mechanism and final morphology, the qualitative difference between the underlying arrested structures of the amorphous and crystalline solids must be reflected in the difference between their respective Debye–Waller factors, $f(q,\infty)$. In other words, the ergodicity restoring processes, identified here, must eventually disrupt the arrested structure irreversibly to such an extent that the structure that evolves is able to support elastic modes not supported by the glass. In the course of the present measurements the samples remain visibly amorphous and, more specifically, $f(q,\infty)$ remains fixed. In this sense, our observations apply to early stage aging.

Strictly speaking then, irreversible processes—processes that drive crystallization—enter gradually when the volume fraction exceeds the freezing value, ϕ_f. As proposed elsewhere,[12] on the strength of analyses of both coherent and incoherent ISFs of these suspensions in the metastable region ($\phi_f<\phi<\phi_g$), irreversible processes are activated when the (partial) arrest of number density fluctuations prevents the dissipation of thermal energy by normal, viscous flow. Moreover, the analysis of the correlation function of the particle currents indicates that in the metastable region, the particle motions cease to be strictly Brownian.[29] As ϕ is increased beyond ϕ_f, the spread of spatial scales closed to viscous dissipation of thermal energy increases. So, the undissipated thermal energy—potential activation energy—increases as, with increasing ϕ, structural relaxation becomes increasingly frustrated. A crossover is reached where (reversible) structural processes have become so frustrated and, concomitantly, the activation energy has become so large, that at least the final decay of the ISF is dominated by irreversible processes. In these suspensions this crossover occurs over a narrow range of volume fractions around $\phi_g \approx 0.565$.

[1] See reviews: L. Cipelletti and L. Ramos, J. Phys.: Condens. Matter **17**, R253 (2005); R. Bandyopadhyay, D. Liang, J. L. Harden, and R. L. Leheny, Solid State Commun. **139**, 589 (2006).
[2] L. Cipelletti, L. Ramos, S. Manley, E. Pitard, D. A. Weitz, E. E. Pashkovski, and M. Johansson, Faraday Discuss. **123**, 237 (2003).
[3] W. Kob and J.-L. Barrat, Eur. Phys. J. B **13**, 319 (2000).
[4] A. M. Puertas, J. Phys.: Condens. Matter **22**, 104121 (2010).
[5] P. N. Pusey and W. van Megen, Nature (London) **320**, 340 (1986).
[6] P. N. Pusey and W. van Megen, Phys. Rev. Lett. **59**, 2083 (1987); W. van Megen and P. N. Pusey, Phys. Rev. A **43**, 5429 (1991).
[7] P. N. Pusey and W. van Megen, Physica A **157**, 705 (1989); P. N. Pusey, Macromol. Symp. **79**, 17 (1994).
[8] W. Götze, *Complex Dynamics of Glass-Forming Liquids. A Mode-Coupling Theory* (Oxford Science, Oxford, 2009).
[9] W. van Megen and S. M. Underwood, Phys. Rev. E **49**, 4206 (1994).
[10] W. van Megen, Phys. Rev. E **76**, 061401 (2007).
[11] H. Z. Cummins, J. Phys.: Condens. Matter **11**, A95 (1999); S. P. Das, Rev. Mod. Phys. **76**, 785 (2004); F. Weysser, A. M. Puertas, M. Fuchs, and Th. Voigtmann, Phys. Rev. E **82**, 011501 (2010).
[12] W. van Megen, V. A. Martinez, and G. Bryant, Phys. Rev. Lett. **102**, 168301 (2009).
[13] J. Müller and T. Palberg, Prog. Colloid Polym. Sci. **100**, 121 (1996).
[14] W. van Megen, T. C. Mortensen, S. R. Williams, and J. Müller, Phys. Rev. E **58**, 6073 (1998).
[15] V. A. Martinez, G. Bryant, and W. van Megen, Phys. Rev. Lett. **101**,

135702 (2008).
[16] S. M. Underwood and W. van Megen, Colloid Polym. Sci. **274**, 1072 (1996).
[17] G. Bryant, S. Martin, A. Budi, and W. van Megen, Langmuir **19**, 616 (2003).
[18] G. Bryant, L. Qian, I. K. Snook, E. Perez, and F. Pincet, Phys. Rev. E **66**, 060501(R) (2002).
[19] M. Fasolo and P. Sollich, Phys. Rev. E **70**, 041410 (2004).
[20] P. N. Pusey, E. Zaccarelli, C. Valeriani, E. Sanz, W. C. K. Poon, and M. E. Cates, Philos. Trans. R. Soc. London, Ser. A **367**, 4993 (2009).
[21] For a critical comparison of the techniques first introduced to deal with nonergodicity see K. Schätzel, Appl. Opt. **32**, 3880 (1993).
[22] L. Cipelletti, H. Bissig, V. Trappe, P. Ballesta, and S. Mazoyer, J. Phys.: Condens. Matter **15**, S257 (2003).
[23] K. N. Pham, S. U. Egelhaaf, A. Moussaid, and P. N. Pusey, Rev. Sci. Instrum. **75**, 2419 (2004).
[24] M. Medebach, M. Dulle, and O. Glatter, J. Phys.: Condens. Matter **21**, 504111 (2009).
[25] W. van Megen, S. M. Underwood, and P. N. Pusey, Phys. Rev. Lett. **67**, 1586 (1991).
[26] P. van Beurten and A. Vrij, J. Chem. Phys. **74**, 2744 (1981).
[27] W. van Megen and S. M. Underwood, Nature (London) **362**, 616 (1993).
[28] J. X. Zhu, M. Li, R. Rogers, R. H. Ottewill, W. B. Russell, and P. M. Chaikin, Nature (London) **387**, 833 (1997).
[29] W. van Megen, V. A. Martinez, and G. Bryant, Phys. Rev. Lett. **103**, 258302 (2009).